Granular metallicity as a minimal normal state for superconductivity

Mingyang Qin,[1,2,*] Xingyu Jiang,[1,2,*] Liping Zhang,[1] Ruozhou Zhang,[1,2] Fucong Chen,[1,2] Juan Xu,[1] Zhongxu Wei,[1,2] Peiyu Xiong,[1] Xu Zhang,[1,2] Li Xu,[1,2] Jie Yuan,[1,3] Beiyi Zhu,[1] Qihong Chen,[1,†] Brigitte Leridon,[4,‡] Kui Jin,[1,2,3,§] and Zhongxian Zhao[1,2,3]

[1]*Beijing National Laboratory for Condensed Matter Physics, Institute of Physics, Chinese Academy of Sciences, Beijing 100190, China*

[2]*School of Physical Sciences, University of Chinese Academy of Sciences, Beijing 100049, China*

[3]*Songshan Lake Materials Laboratory, Dongguan, Guangdong 523808, China*

[4]*LPEM, ESPCI Paris, PSL Research University, CNRS, Sorbonne Université, 75005 Paris, France*

(Received 30 June 2021; revised 28 October 2021; accepted 5 November 2021; published 17 November 2021)

We report the evolution of electrical transport properties in insulating FeSe films with electron doping induced by the ionic liquid gating technique. Superconductivity never emerges in the strong insulators with variable-range hopping behavior but is shown to arise once the resistance of the normal state varies as $\ln(1/T)$, indicating that this behavior corresponds to the minimal conducting character for developing superconductivity. Our work points toward granular metallicity for the $\ln(1/T)$ behavior, suggesting that the emergence of superconductivity requires at least an insulating state containing metallic granules. Moreover, it unravels an electronic segregation in proximity to superconductor-insulator transition, which calls for a comprehensive understanding of this segregated phase.

DOI: 10.1103/PhysRevB.104.174511

I. INTRODUCTION

The quantum superconductor-insulator transition (QSIT) in two-dimensional (2D) systems is believed to be an important example of a quantum phase transition, which occurs at zero temperature when the ground state of a system is altered by varying an external parameter of the Hamiltonian, such as the magnetic field, the level of disorder, or the carrier density [1,2]. In past decades, great efforts have been made to investigate the quantum criticality at the transition between insulating and superconducting ground states [3,4]. In most cases, there is a clear horizontal separatrix between downward and upward resistance-versus-temperature curves, marking the existence of a well-defined quantum critical point and enabling one to extract scaling laws associated with the critical exponents [5]. Actually, most of the tuning parameters modify not only the superconducting ground state but also the normal state. However, very few studies focus on the evolution of normal-state transport properties with the tuning parameter. There is still no conclusive answer to an important question, namely, what is the minimal condition on the nature of the normal state for superconductivity to develop, which is in particular of vital importance to understand the interplay between localization and superconductivity [6].

BCS theory requires the existence of a well-defined Fermi surface for the superconducting instability to take place, but many materials with a negative temperature coefficient for resistance in the normal state exhibit superconductivity below a finite critical temperature (T_c). In the literature, while variable-range hopping (VRH)-dominated granular materials have been claimed to be low-temperature superconductors [7,8], superconductivity is more often associated with an enigmatic $\ln(1/T)$ behavior [9–13].

In order to address this issue, a quasicontinuous tuning of the normal state is in great demand. However, the conventional approaches, which include changing the film thickness, applying a magnetic field, chemical doping, or thermal annealing, can introduce several simultaneous effects [14]. For instance, changing the film thickness alters the level of disorder by reducing the mean free path but may also change the material structure. Magnetic fields inevitably introduce vortices and the related complex vortex physics. Chemical doping may change the carrier density and the disorder. And thermal annealing may involve variation in both morphology and chemical composition. By contrast, the ionic liquid gating technique (ILG) varies essentially the carrier density and only marginally other parameters [15]. More importantly, it enables one to realize a continuous tuning of the carrier doping by virtue of the electrostatic or electrochemical effects [16], which is conducive to studying the emergence of superconductivity in detail [17–19].

Here, we employed ILG to modify the electron doping in initially insulating FeSe thin films and systematically investigated the evolution of electrical transport properties, seeking the necessary condition for emergence of superconductivity. It is found that the insulativity of the samples gradually weakens with electron doping. For the strong insulators with VRH behavior, superconductivity does not develop in our measuring temperature range. On the contrary, superconducting fluctuations are shown to arise as soon as the resistance at low temperatures varies as $\ln(1/T)$, indicating a minimal condition on the normal-state conductivity for superconductivity to

*These authors contributed equally to this work.
†Corresponding author: qihongchen@iphy.ac.cn
‡Corresponding author: brigitte.leridon@espci.fr
§Corresponding author: kuijin@iphy.ac.cn

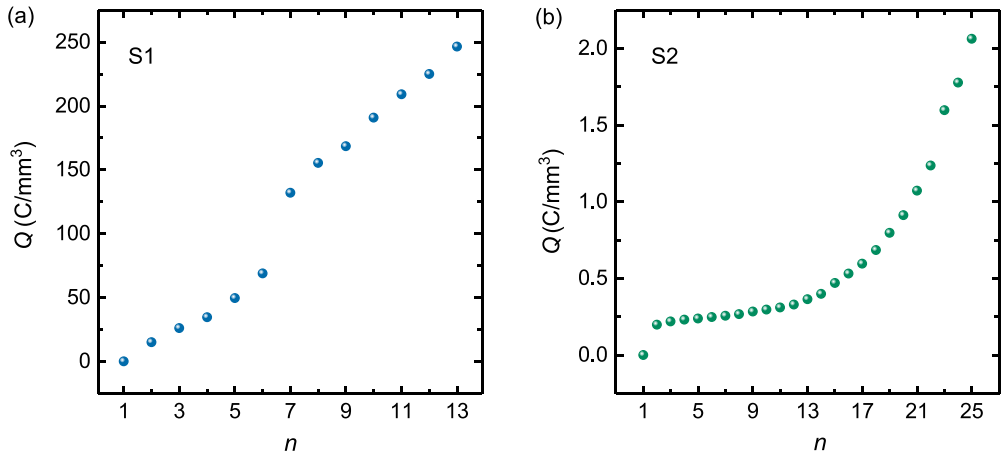

FIG. 1. Amount of doped charge versus gating sequence for samples (a) S1 and (b) S2.

develop. We attribute this $\ln(1/T)$ behavior to granular metallicity, which may originate from either structural granularity or spontaneous electronic segregation.

II. EXPERIMENTS

The β-FeSe films, S1, S2, and S3, were grown on (001)-oriented CaF_2 substrates by pulsed laser deposition system equipped with a 248-nm KrF excimer laser [20]. The polycrystalline targets were prepared by the solid-state reaction method. The laser repetition rate was 4 Hz and the base vacuum of deposition chamber was 10^{-7} torr. The film thicknesses were typically of several hundred nanometers. For S1, S2, and S3, the substrate temperatures were 300, 350, and 350 °C, respectively; The laser energies were 250, 250, and 350 mJ, respectively. S3 has been annealed under 400 °C for 1 h after deposition. X-ray diffraction (XRD) data were obtained using a SmartLab diffractometer with a Ge (220) crystal monochromator. The energy dispersive x-ray spectra (EDX) and microstructure measurements were performed with a Hitachi SU5000 field-emission scanning electron microscope (SEM).

The ILG experiments were performed on insulating samples S1 and S2 using a homemade device [21], which was mounted on the 3-K platform of the commercial Montana Instruments cryocooler and allowed simultaneous *in situ* resistance and magnetic measurements. The ionic liquid, *N*, *N*-diethyl-*N*-methyl-*N*-(2-methoxyethyl) ammonium bis(trifluoromethylsulphonyl)imide, was used as the dielectric, covering the FeSe film and the Au gate electrode. A Keithley 2400 source meter was used to apply the gate voltage and monitor the leakage current. The resistance was measured in a four-terminal configuration with a Keithley 6221 current source meter and a Keithley 2182 voltage meter. The *in situ* magnetic measurements were performed using a two-coil mutual inductance technique. A Stanford Research SR830 lock-in amplifier with a reference phase of 90° was used to apply an alternative current to the drive coil. The current had a frequency of 50 kHz and an amplitude of 0.2 mA. The same lock-in amplifier was used to measure the induced voltage in the pickup coil, $V = V_x - iV_y$, where V_x reflects the diamagnetism of samples and the full width at half maximum of V_y is a measure of the homogeneity of the superconducting state.

A complete gating experiment consists of many sequences, each of which involves (i) warming up to a target temperature under an appropriate gate voltage. (ii) staying at the target temperature for a given period of time, and (iii) cooling down to the base temperature and, meanwhile, measuring the temperature dependence of the resistance and the magnetic response. With careful adjustment of the gate voltage, the gating temperature, and the duration time, we were able to realize a quasicontinuous electrochemical doping of electron carriers [22]. The amount of doped charge for each gating sequence (n), denoted as Q, was estimated as the temporal integral of the leakage current [23]. The correspondences between n and Q for S1 and S2 are shown in Fig. 1. Note that the calculated Q tends to overestimate the actual amount of carriers injected into the sample since the leakage current is contributed not only by the doping effect, but also affected by other factors such as electrochemical reaction and electric leakage in the system. These effects are more prominent in S1. In our experiment, the ILG data are not reversible; i.e., the sample does not return to the pristine state after the gate voltage is removed. This indicates that the gating process is mainly electrochemical rather than purely electrostatic.

III. RESULTS AND DISCUSSIONS

A. Mechanisms of insulativity in FeSe films

Figure 2(a) shows the sheet resistance (R_s) versus the temperature (T) of two insulating FeSe films, S1 and S2, and one superconducting film, S3 ($T_c \sim 8$ K). The insulating behavior in FeSe was attributed to the lattice strain in previous work [24]. In the present case, this mechanism can be ruled out since the insulating and superconducting samples show almost identical XRD patterns as shown in Fig. 2(b). Instead, the EDX reveals that the atomic ratios of Fe to Se in the insulating samples are lower than that in the superconducting sample. Hence, we infer that the insulativity in our FeSe films originates from Fe vacancies, which is consistent with previous reports [25,26].

Actually, there are evident distinctions between the two insulating samples. For the strongly insulating sample S1, the resistance monotonically increases with decreasing temperature and the data between 20 and 100 K can be

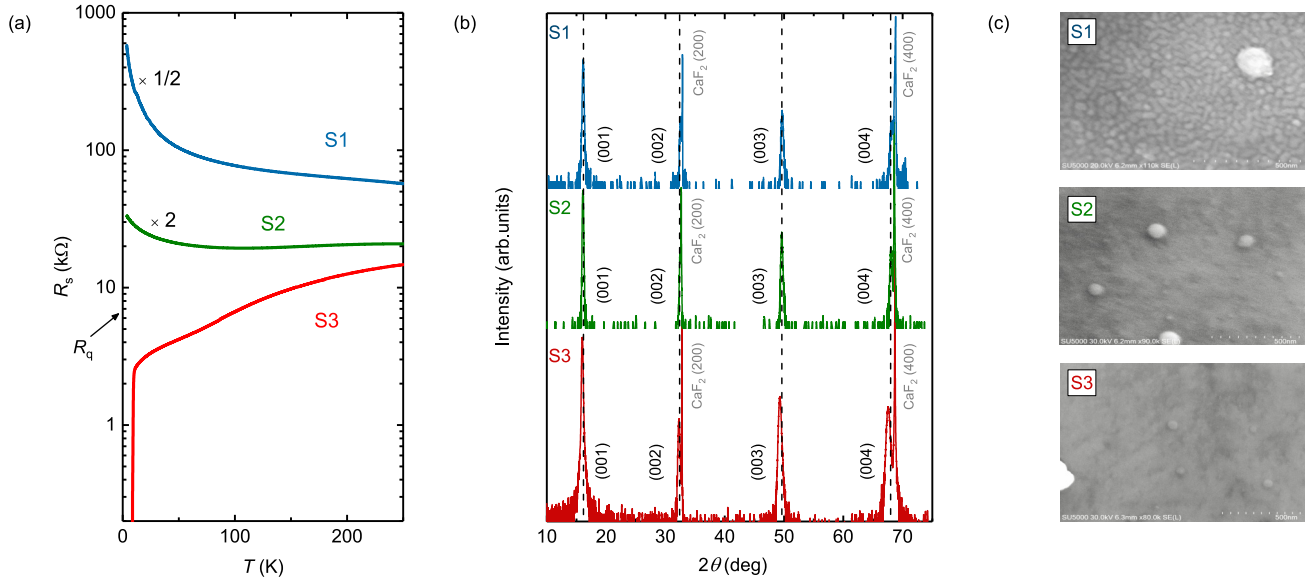

FIG. 2. Electrical transport properties, crystalline structure, and microstructure for samples S1, S2, and S3. (a) Sheet resistance versus temperature curves. R_q at the longtudinal axis is the pair quantum resistance [5]. (b) Out-of-plane XRD patterns. (c) SEM micrographs.

well fitted by the 2D VRH formula [27], namely, $R_s = R_{s0}\exp[(T_0/T)^{1/3}]$, where T_0 is in inverse proportion to the localization length. For the weakly insulating sample S2, as the temperature decreases, the resistance first decreases at high temperatures, reaches a minimum at ∼100 K, and then starts to increase as $\ln(1/T)$ at lower temperatures. The fits are shown in Fig. 3. In addition, SEM demonstrates that S1 exhibits some structural granularity with a typical granule size of ∼50 nm, while S2 is structurally homogeneous [see Fig. 2(c)].

B. Minimal condition for superconductivity

Figure 4(a) pictures the sheet resistance versus temperature for gating sequences Nos. 1–13 of sample S1, where sequence 1 corresponds to the pristine state. The curves are normalized to the sheet resistance at 250 K. From sequence 1 to sequence 7, the sample remains strongly insulating and the data below ∼100 K could always be well fitted using $R_s = R_{s0}\exp[(T_0/T)^{1/3}]$ [see Fig. 4(b)]. The extracted T_0 is found to rapidly decrease with doping [see Fig. 4(d)], pointing to a decreasing distance between hopping sites and indicating a weakening of the insulativity [28]. Intriguingly, for sequence 8 and beyond, a minimum appears in the $R_s(T)$ curves, indicating a metallic behavior at high temperatures. The position of this minimum is denoted by T_{min} in Fig. 4(d). Simultaneously, the resistance at low temperatures ceases to be VRH-dominated and instead varies as $\ln(1/T)$ [see Fig. 4(c)].

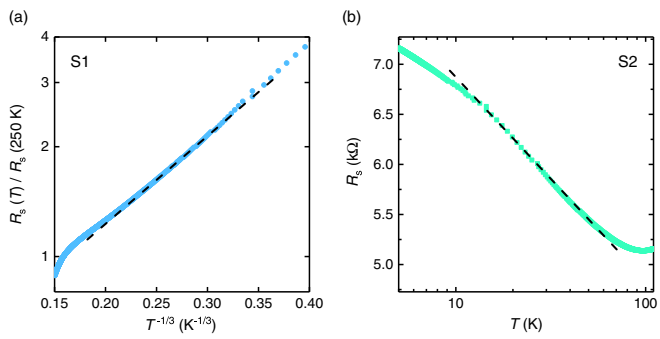

FIG. 3. (a) Normalized sheet resistance (on a log scale) versus $T^{-1/3}$ for pristine S1. The dashed line is the linear fitting result. (b) Sheet resistance R_s as a function of temperature T (on a log scale) for pristine S2. The linear regime (dashed line) shows that the resistance varies as $\ln(1/T)$.

After a given threshold in the charge injected into the system ($Q \sim 190$ C/mm^3), superconductivity appears. In order to track the appearance of superconductivity, we extracted the inflexion point at low temperatures (see Appendix A), which is used to mark the onset of superconducting fluctuations [29]. It is worth mentioning that more methods are needed to accurately determine the onset temperature of superconducting fluctuations [30–33]. The temperature at the inflexion point, T_{inf}, is plotted in Fig. 4(d). Note that for gating sequences 8 and 9, there is already a departure from the logarithmic behavior below 6 K [see Fig. 4(c)]. This tends to indicate that as soon as VRH behavior yields to $\ln(1/T)$ behavior and the resistance minimum appears, the system becomes superconducting at low temperatures. In other words, the $\ln(1/T)$ resistance appears as a minimal condition on the normal-state conductivity for superconductivity to develop.

This $\ln(1/T)$ behavior seems at first evocative of weak localization [34,35] but, after inspection, cannot be explained in this way since (i) the logarithm correction in our data is too important [the resistance increases as $\ln(1/T)$ by typically 50 to 100%] and besides, (ii) the correction to conductance does not follow a logarithm variation as expected for weak localization (see Fig. 5). As a matter of fact, such a $\ln(1/T)$ variation is often encountered in the vicinity of QSIT in high-T_c cuprates [9–11] and in granular low-T_c superconductors [12,13,36]. Accordingly, theories based either on Bose metal physics [37,38] or on granular metallicity [39,40] have been developed to account for this $\ln(1/T)$ behavior. Given that the pristine S1 is found to be structurally granular [see Fig. 2(c)], it is tempting to conclude that the $\ln(1/T)$ behavior results

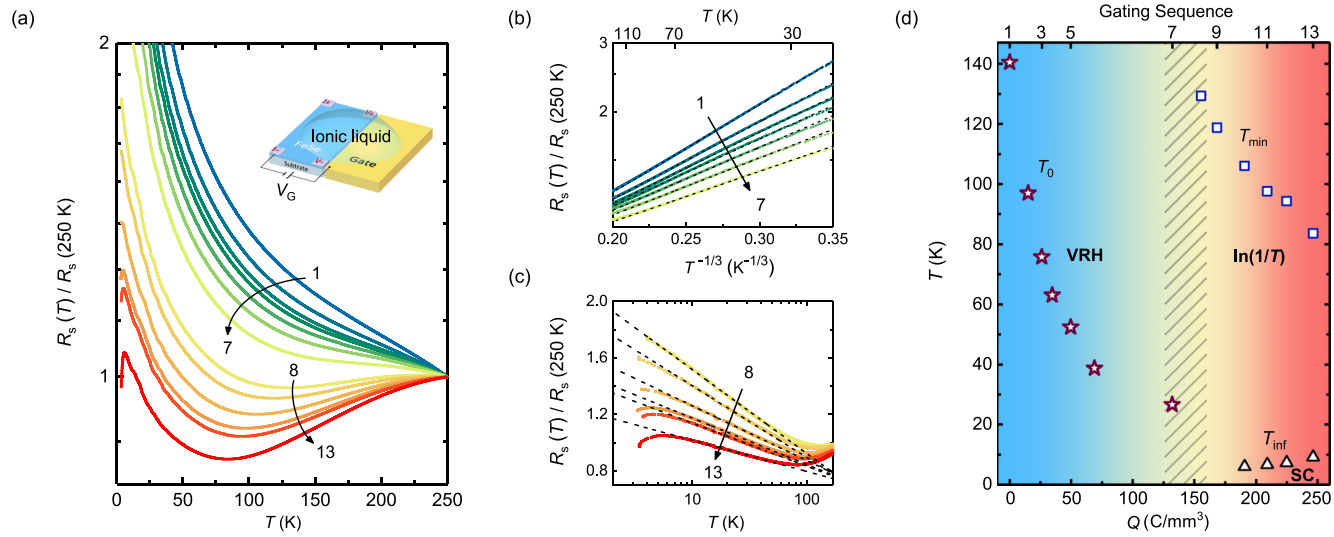

FIG. 4. Evolution of electrical transport properties with Q for sample S1. (a) Temperature dependence of the normalized sheet resistance for gating sequences Nos. 1–13. The inset shows the schematic of the ILG device. (b) Logarithm of the normalized sheet resistance versus $T^{-1/3}$ for sequences 1–7. (c) Normalized sheet resistance versus logarithm of T for sequences 8–13. The dashed lines in panels (b) and (c) are the results of linear fitting. (d) T_0 (open stars) extracted from the fit in panel (b), $T_{\min}$ (open squares), and $T_{\inf}$ (open triangles) as a function of Q. The shading marks the crossover from VRH behavior to $\ln(1/T)$ resistance, compatible with superconductivity (SC).

from granular metallicity, emerging in this case from the structural inhomogeneities. Such a mild insulator (or more precisely a granular metal), where metallic granules hosting superconductivity are embedded in an insulating matrix, would therefore constitute the minimal normal state that can support superconductivity in this system.

C. Proofs of electronic granularity

Interestingly enough, we note that the pristine weakly insulating sample S2 exhibits both $\ln(1/T)$ behavior and resistance minimum in qualitative agreement with the resistance found during sequence 8 of sample S1 (see Fig. 3), which tends to indicate here also the existence of electronic granularity in S2, while the system is not structurally granular as is attested by the SEM image in Fig. 2(c). In order to deeper explore the behavior of S2, an elaborate ILG experiment was performed. Figure 6(a) shows the sheet resistance versus temperature for gating sequences 1–25. It is found that both metallicity and superconductivity of the sample are enhanced with increasing Q. To depict the evolution of resistance curves, several characteristic temperatures are plotted in Fig. 6(c), where T_{c0} and $T_{c,MF}$ represent the zero-resistance critical temperature and mean-field critical temperature, respectively. (Definitions of characteristic temperatures can be found in Appendix A). Remarkably, a $T_{\inf}$ above 20 K is already seen in sequence 2 ($Q \sim 0.2$ C/mm^3), indicating the pristine S2 is on the verge of the superconducting state. As a matter of fact, R_q, the pair quantum resistance, separates sequences 1 and 2. This suggests that for sample S2, the $\ln(1/T)$ resistance also corresponds to a normal state compatible with superconductivity.

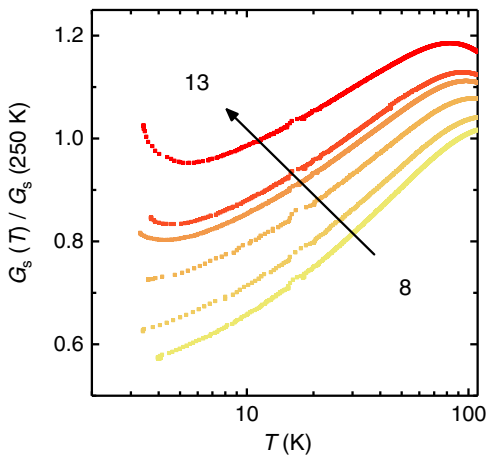

FIG. 5. Normalized sheet conductance versus logarithm of temperature for gating sequences 8–13 of S1. There is no linear regime in this plot.

Figure 6(b) enables us to follow the diamagnetic response of the sample with gating, measured by the two-coil mutual inductance technique [41] with sample sandwiched between two coils [see the schematic in Fig. 6(a)]. The V_x at 5 K, denoted as VF in Fig. 6(c), is used to estimate the volume fraction of the superconducting phase. It shows that the diamagnetic screening becomes stronger and progressively covers the whole fraction of the sample. For the first few gating sequences, VF is nearly zero but $T_{c,MF}$ is sizable, indicating that a well-established superconducting phase takes place on a very small fraction of the volume. The well-defined $T_{c,MF}$ in the absence of T_{c0} is in favor of a granular picture where superconducting granules are embedded in an insulating background. The following increase of VF points to growing of superconducting granules with doping. When VF increases to a sufficient level, T_{c0} appears (sequence 16 marked by dotted lines in Fig. 6), which means that the superconductivity becomes fully percolated.

Furthermore, we tentatively investigated the superconducting fluctuations for the system before and after percolation.

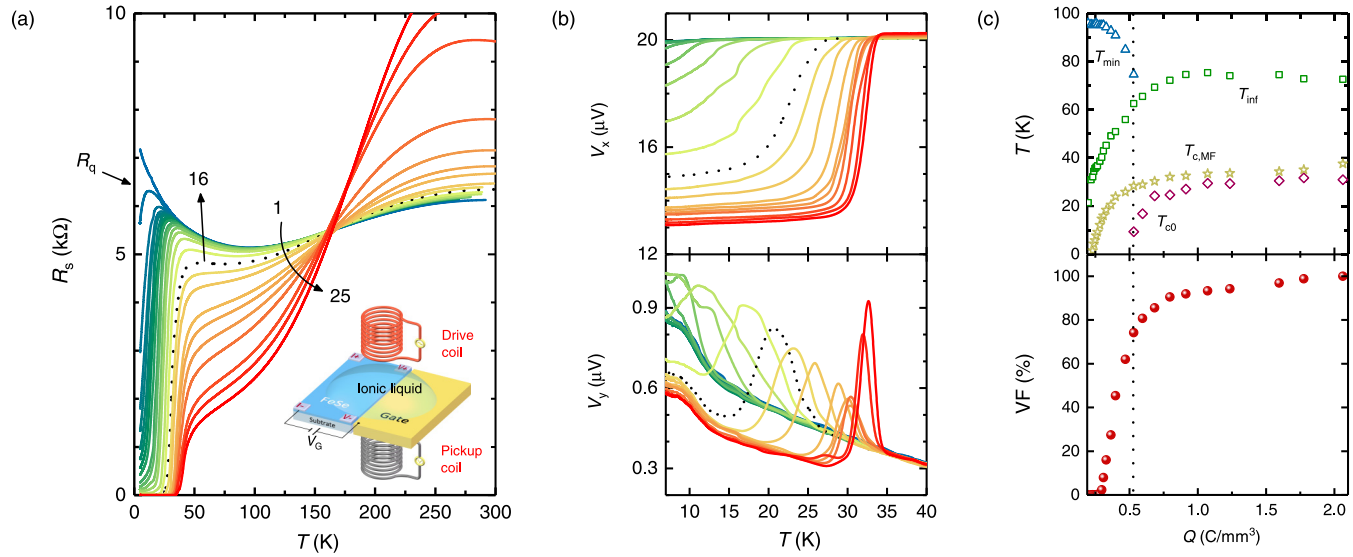

FIG. 6. Evolution of electrical transport properties and diamagnetic responses with Q for sample S2. (a) Temperature dependence of sheet resistance for gating sequences 1–25. The inset shows the schematic of the homemade device. R_q separates upward and downward curves at low temperatures. (b) The induced voltage in the pickup coil as a function of T for sequences 1–25. V_x and V_y are the real and imaginary components of the pickup voltage, respectively. (c) T_{min} (open triangles), T_{inf} (open squares), $T_{c,MF}$ (open stars), T_{c0} (open diamonds), and VF (solid circles) as a function of Q, where the VF for sequence n is defined as $[V_x(n) - V_x(1)]/V_x(25)$ at 5 K. The dotted lines correspond to sequence 16.

We extracted the sheet pararesistance ΔG_s^{-1} for sequences 10 (before percolation) and 25 (after percolation), where ΔG_s is the sheet paraconductance. The details are described in Appendix B. As shown in Fig. 7, there are indeed a clear 0D Aslamasov-Larkin (AL) [42] regime before percolation and a 2D AL regime after percolation, with a possible 0D/2D crossover in the latter case, which could be reminiscent of electronic inhomogeneities (see the schematics in Fig. 7). These findings additionally point toward the existence of electronic granularity in S2 [36]. Note that more methods than dc resistivity measurement are needed to quantitatively describe the superconducting fluctuations [43].

In addition, it is worth mentioning that all the resistance-versus-temperature curves intersect at ∼164 K in Fig. 6(a) for S2. Such a crossing point was systematically observed in our gating experiments on different samples (see Appendix C) and was already reported in previous work [19,44]. Here, we suggest a possible explanation based on doping-induced interchange between two types of carriers. We assume that there are two types of carriers whose densities, n_1 and n_2, contain a part that varies linearly with Q, with respective coefficients A and B. Then there will exist a crossing point located at the temperature T^* for which $A/B = -\tau_2(T^*)m_1/\tau_1(T^*)m_2$, where τ and m represent the relaxation time and the effective

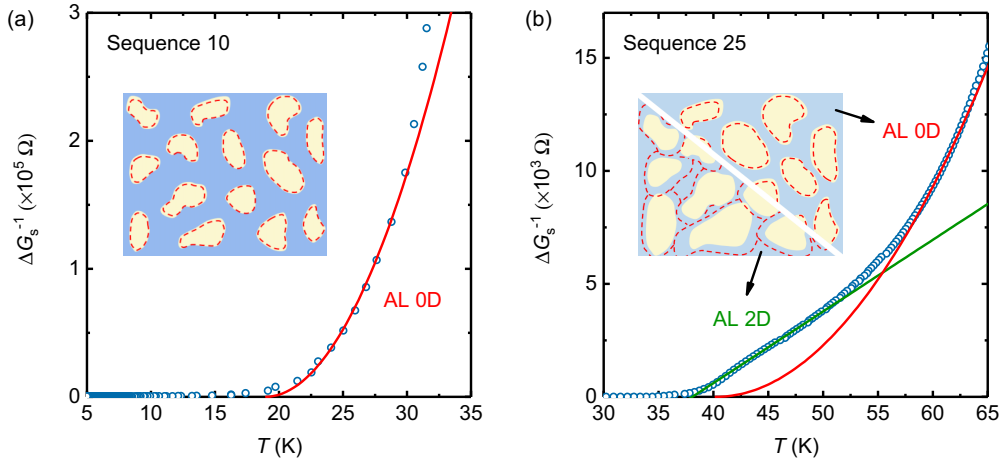

FIG. 7. Sheet pararesistance ΔG_s^{-1} as a function of T for (a) sequence 10 (before percolation) and (b) sequence 25 (after percolation) of sample S2. The red and green solid lines are the fitting results with the 0D [$\Delta G_s^{-1} \propto (T - T_{c,0D})^2$] and 2D ($\Delta G_s^{-1} \propto T - T_{c,2D}$) AL formulas, respectively, where $T_{c,0D}$ and $T_{c,2D}$ are fluctuational critical temperatures [36]. The insets display schematics of the spatial distribution of the electronic states close to T_c, where the metallic granules (yellow) hosting superconducting fluctuations (red dashed lines) are embedded in an insulating matrix (blue) before percolation and in a weak insulator (or a bad metal, light blue) after percolation. The presence of the 0D regime in the latter case illustrates the persistence of the electronic inhomogeneities.

mass, respectively. Additional details are described in Appendix C. The negative A/B is a strong indication that doping acts in an opposite way on the two types of carriers. The question of whether these two types of carriers are separated in real space (segregation) or in k-space (corresponding to different pockets of the Fermi surface) cannot be elucidated at this point. Of course it is tempting here to relate these two types of carriers to the granularity of the electronic system. In this case, doping on this segregated electronic system changes the balance between the insulating region and the metallic granules hosting superconductivity, in favor of the latter. As a result, the superconducting granules grow while the insulating region shrinks with doping, which is consistent with the picture shown in the insets of Fig. 7.

All above analyses point to electronic granularity in pristine S2, implying that the $\ln(1/T)$ behavior also stems from the granular metallicity. In view of its homogeneous structure [see Fig. 2(c)], we attribute this granularity to an electronic phase segregation. The question remains of whether this segregation is a genuine property of the metallic phase itself or whether it is due to the proximity of an inhomogeneous superconducting phase, which can emerge from homogeneously disordered films [36,45,46]. Besides, it is to be noted that more recently, the $\ln(1/T)$ resistance has been associated experimentally with the presence of charge density waves in cuprates [29,47], which is also a form of electronic segregation.

IV. CONCLUSIONS

In summary, through ILG experiments on two different insulating FeSe films, we successfully established the existence of a minimal condition on the conductivity of normal-state supporting superconductivity, corresponding to $\ln(1/T)$ resistance. It is presumably related to granular metallicity, which results in the first sample from preexisting structural granularity and in the second sample from electronic segregation. This work tends to question whether superconductivity is really able to develop from a truly insulating normal state and to establish that it requires at least an insulating state containing metallic granules. It should be emphasized that such correlation between $\ln(1/T)$ behavior of the normal-state resistance and superconductivity also exists in low-T_c superconductors [12] and seems to be present as well in some high-T_c cuprates [48]. This subsequently raises the question of the universality of this relationship. In addition, it has been revealed that the electronic segregation mechanism may make QSIT unconventional [48], which calls for a more comprehensive theory on this granular electronic state and its interplay with superconductivity.

ACKNOWLEDGMENTS

We thank Sergio Caprara, Hongyi Xie, Jiangping Hu, Luca d' Medici, and Tommaso Gorni for fruitful discussions. This work was supported by the National Key Basic Research Program of China (Grants No. 2017YFA0302902, No. 2017YFA0303003, and No. 2018YFB0704102), the National Natural Science Foundation of China (Grants No. 11927808, No. 11834016, No. 118115301, No. 119611410, and No. 11961141008), the Key Research Program of Frontier Sciences, CAS (Grants No. QYZDB-SSW-SLH008 and No. QYZDY-SSW-SLH001), the Strategic Priority Research Program (B) of the Chinese Academy of Sciences (Grants No. XDB25000000 and No. XDB33000000), the Beijing Natural Science Foundation (Grant No. Z190008), the Key-Area Research and Development Program of Guangdong Province (Grant No. 2020B0101340002), and the CAS Interdisciplinary Innovation Team. We also acknowledge the European COST action Nanocohybri (Grant No. CA16218).

APPENDIX A: DEFINITIONS OF CHARACTERISTIC TEMPERATURES

Figure 8 shows the definitions of characteristic temperatures. T_{inf} is defined as the inflexion point of the $R_s(T)$ curve above the onset temperature of superconductivity. $T_{c,MF}$ is defined as the intersection of the tangent at midheight of the superconducting transition with the T axis.

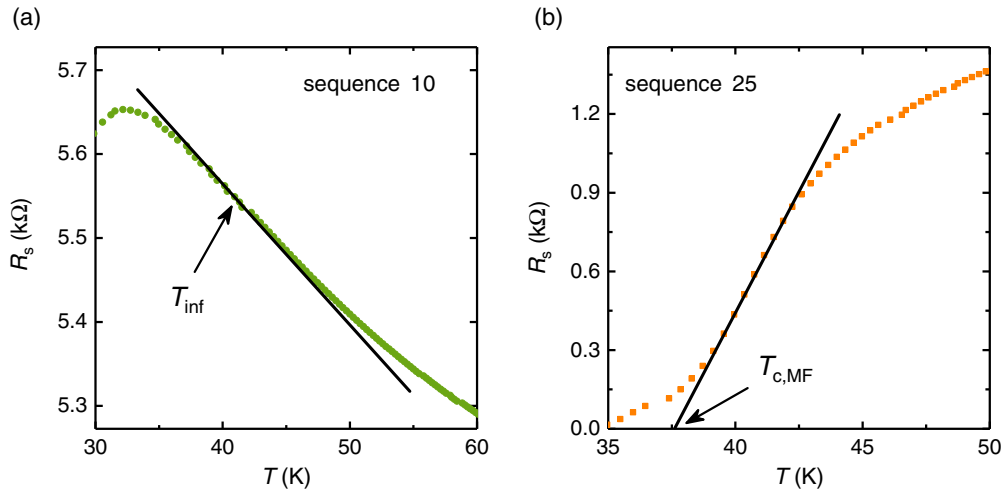

FIG. 8. (a) Zoom-in of the $R_s(T)$ curve for sequence 10 of S2. The arrow indicates the position of T_{inf}. The solid line shows the tangent at the inflexion point. (b) Zoom-in of the $R_s(T)$ curve for sequence 25 of S2. The arrow indicates the position of $T_{c,MF}$. The solid line shows the tangent at midheight of the transition.

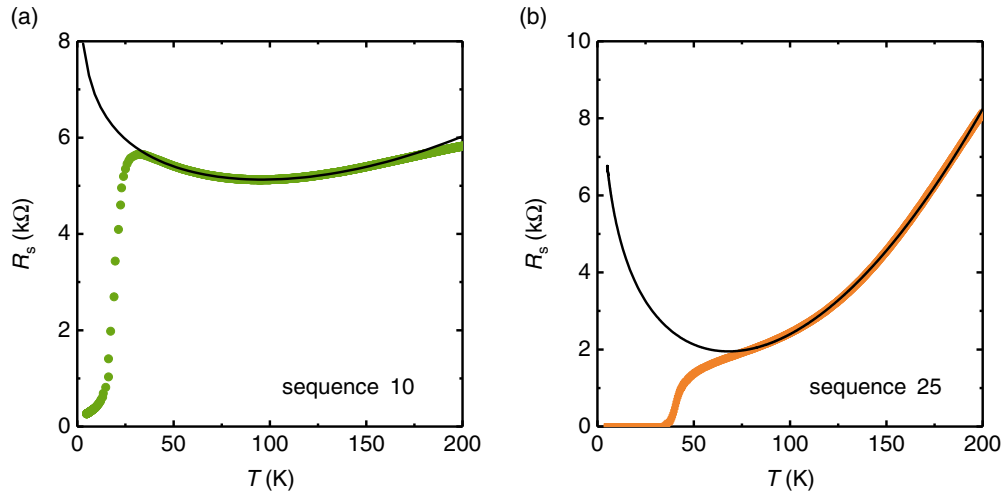

FIG. 9. Sheet resistance R_s as a function of T for (a) sequence 10 and (b) sequence 25 of S2. The solid lines are for the normal-state sheet resistances R_s^n.

APPENDIX B: EXTRACTION OF SHEET PARARESISTANCE

As shown in Fig. 9, the normal-state sheet resistances R_s^n was extrapolated from the experimental data using the fitting law $R_s^n = AT^2 + B\ln(1/T) + C$, with parameters $A = 0.05$ and 0.25, $B = -2196.87$ and -5279.91, and $C = 9005.51$ and 10481.37 for sequences 10 and 25, respectively. In Fig. 7 of the text, the sheet pararesistance is defined as $\Delta G_s^{-1} = (G_s - G_s^n)^{-1} = (1/R_s - 1/R_s^n)^{-1}$. Given the fact that the normal state is extrapolated at low temperatures, it is not possible to perform a reliable quantitative fit of the amplitude of the pararesistance. However, since the normal state does not contain any divergence at T_c, the value of the critical exponents (consistent with either 2D or 0D AL fluctuations) is on the contrary highly reliable. For sequence 10, the fitting parameter $T_{c,0D}$ is 18.9 K. For sequence 25, $T_{c,0D}$ and $T_{c,2D}$ are 40.2 and 38.1 K, respectively.

APPENDIX C: EXPLANATION OF CROSSING POINT

Figure 6(a) shows that for S2 which is initially insulating, the $R_s(T)$ curves with different Q intersect at ∼164 K. Such a crossing phenomenon could be repeated by gating a superconducting sample with a metallic normal state (see Fig. 10). Here, we provide an explanation of the crossing point based on Q-induced interchange between two types of carriers. It is assumed that the electronic system consists of two components with densities n_1 and n_2, which vary linearly with Q, i.e.,

$$n_1(Q) = AQ + n_{10}, \quad n_2(Q) = BQ + n_{20} \tag{C1}$$

where A, B, n_{10}, and n_{20} are constants. Besides, the conductivity σ has the Drude form, i.e.,

$$\sigma(Q,T) = n_1(Q)e^2\tau_1(T)/m_1 + n_2(Q)e^2\tau_2(T)/m_2. \tag{C2}$$

Then

$$\sigma(Q,T) = [A\tau_1(T)/m_1 + B\tau_2(T)/m_2]Qe^2 + [n_{10}\tau_1(T)/m_1 + n_{20}\tau_2(T)/m_2]e^2. \tag{C3}$$

A crossing point located at the temperature T^* means that

$$\partial\sigma(Q,T)/\partial Q|_{T^*} = 0. \tag{C4}$$

Thus,

$$A/B = -\tau_2(T^*)m_1/\tau_1(T^*)m_2. \tag{C5}$$

The negative A/B implies that doping acts in an opposite way on the two types of carriers.

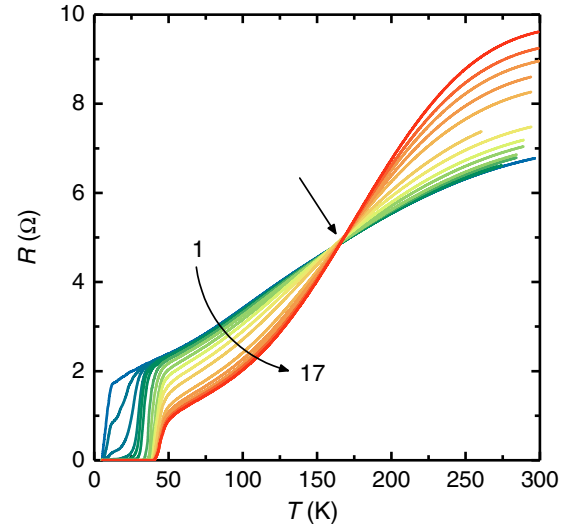

FIG. 10. Temperature dependence of resistance for different gating sequences (1–17). The pristine sample (sequence 1) is a superconductor with a metallic normal state. The arrow indicates the crossing point.

[1] S. L. Sondhi, S. M. Girvin, J. P. Carini, and D. Shahar, Rev. Mod. Phys. **69**, 315 (1997).

[2] S. Sachdev, *Quantum Phase Transitions* (Cambridge University Press, Cambridge, England, 1999).

[3] V. F. Gantmakher and V. T. Dolgopolov, Phys.-Usp. **53**, 1 (2010).

[4] A. M. Goldman, Int. J. Mod. Phys. B **24**, 4081 (2010).

[5] M. P. A. Fisher, Phys. Rev. Lett. **65**, 923 (1990).

[6] R. C. Dynes, J. P. Garno, and J. M. Rowell, Phys. Rev. Lett. **40**, 479 (1978).

[7] Y. Shapira and G. Deutscher, Phys. Rev. B **27**, 4463 (1983).

[8] A. Gerber, A. Milner, G. Deutscher, M. Karpovsky, and A. Gladkikh, Phys. Rev. Lett. **78**, 4277 (1997).

[9] G. S. Boebinger, Y. Ando, A. Passner, T. Kimura, M. Okuya, J. Shimoyama, K. Kishio, K. Tamasaku, N. Ichikawa, and S. Uchida, Phys. Rev. Lett. **77**, 5417 (1996).

[10] S. Ono, Y. Ando, T. Murayama, F. F. Balakirev, J. B. Betts, and G. S. Boebinger, Phys. Rev. Lett. **85**, 638 (2000).

[11] B. Leridon, J. Vanacken, T. Wambecq, and V. V. Moshchalkov, Phys. Rev. B **76**, 012503 (2007).

[12] G. Deutscher, B. Bandyopadhyay, T. Chui, P. Lindenfeld, W. L. McLean, and T. Worthington, Phys. Rev. Lett. **44**, 1150 (1980).

[13] R. W. Simon, B. J. Dalrymple, D. Van Vechten, W. W. Fuller, and S. A. Wolf, Phys. Rev. B **36**, 1962 (1987).

[14] K. A. Parendo, K. H. Sarwa B. Tan, and A. M. Goldman, Phys. Rev. B **73**, 174527 (2006).

[15] H. Yuan, H. Shimotani, A. Tsukazaki, A. Ohtomo, M. Kawasaki, and Y. Iwasa, Adv. Funct. Mater. **19**, 1046 (2009).

[16] X. Wei, H. Li, Q. Zhang, D. Li, M. Qin, L. Xu, W. Hu, Q. Huan, L. Yu, J. Miao, J. Yuan, B. Zhu, A. Kusmartseva, F. V. Kusmartsev, A. V. Silhanek, T. Xiang, W. Yu, Y. Lin, L. Gu, P. Yu, Q. Chen, and K. Jin, Sci. Bull. **65**, 1607 (2020).

[17] X. Leng, J. Garcia-Barriocanal, S. Bose, Y. Lee, and A. M. Goldman, Phys. Rev. Lett. **107**, 027001 (2011).

[18] A. T. Bollinger, G. Dubuis, J. Yoon, D. Pavuna, J. Misewich, and I. Bozovic, Nature (London) **472**, 458 (2011).

[19] K. Hanzawa, H. Sato, H. Hiramatsu, T. Kamiya, and H. Hosono, Proc. Natl. Acad. Sci. USA **113**, 3986 (2016).

[20] Z. Feng, J. Yuan, G. He, W. Hu, Z. Lin, D. Li, X. Jiang, Y. Huang, S. Ni, J. Li, B. Zhu, X. Dong, F. Zhou, H. Wang, Z. Zhao, and K. Jin, Sci. Rep. **8**, 4039 (2018).

[21] M. Qin, R. Zhang, Z. Lin, Z. Feng, X. Wei, S. Blanco Alvarez, C. Dong, A. V. Silhanek, B. Zhu, J. Yuan, Q. Qin, and K. Jin, J. Supercond. Nov. Magn. **33**, 159 (2020).

[22] X. Zhang, Z. Feng, X. Wei, Z. Lin, X. Jiang, W. Hu, Z. Wei, M. Qin, J. Xu, R. Xiong, J. Shi, J. Yuan, B. Zhu, Q. Chen, and K. Jin, Phys. Rev. B **103**, 214505 (2021).

[23] Z. Wei, Q. Li, B. C. Gong, X. Wei, W. Hu, Z. Ni, G. He, M. Qin, A. Kusmartseva, F. V. Kusmartsev, J. Yuan, B. Zhu, Q. Chen, J. H. Chen, K. Liu, and K. Jin, Phys. Rev. B **103**, L140501 (2021).

[24] K. Hanzawa, Y. Yamaguchi, Y. Obata, S. Matsuishi, H. Hiramatsu, T. Kamiya, and H. Hosono, Phys. Rev. B **99**, 035148 (2019).

[25] T. K. Chen, C. C. Chang, H. H. Chang, A. H. Fang, C. H. Wang, W. H. Chao, C. M. Tseng, Y. C. Lee, Y. R. Wu, M. H. Wen, H. Y. Tang, F. R. Chen, M. J. Wang, M. K. Wu, and D. Van Dyck, Proc. Natl. Acad. Sci. USA **111**, 63 (2014).

[26] K. Yeh, Y. Chen, T. Lo, P. M. Wu, M. Wang, K. Chang-Liao, and M. Wu, Front. Phys. **8**, 567054 (2020).

[27] N. F. Mott, Philos. Mag. **19**, 835 (1987).

[28] R. Schneider, A. G. Zaitsev, D. Fuchs, and H. v. Löhneysen, Eur. Phys. J. B **88**, 14 (2015).

[29] S. Caprara, M. Grilli, J. Lorenzana, and B. Leridon, SciPost Phys. **8**, 003 (2020).

[30] S. Kasahara, T. Yamashita, A. Shi, R. Kobayashi, Y. Shimoyama, T. Watashige, K. Ishida, T. Terashima, T. Wolf, F. Hardy, C. Meingast, H. V. Lohneysen, A. Levchenko, T. Shibauchi, and Y. Matsuda, Nat. Commun. **7**, 12843 (2016).

[31] H. Takahashi, F. Nabeshima, R. Ogawa, E. Ohmichi, H. Ohta, and A. Maeda, Phys. Rev. B **99**, 060503(R) (2019).

[32] T. Hanaguri, S. Kasahara, J. Boker, I. Eremin, T. Shibauchi, and Y. Matsuda, Phys. Rev. Lett. **122**, 077001 (2019).

[33] Y. Mizukami, M. Haze, O. Tanaka, K. Matsuura, D. Sano, J. Böker, I. Eremin, S. Kasahara, Y. Matsuda, and T. Shibauchi, arXiv:2105.00739.

[34] E. Abrahams, P. W. Anderson, D. C. Licciardello, and T. V. Ramakrishnan, Phys. Rev. Lett. **42**, 673 (1979).

[35] L. P. Gorkov, A. I. Larkin, and D. E. Khmelnitskii, Pis'ma Zh. Eksp. Teor. Fiz. **30**, 248 (1979) [JETP Lett. **30**, 228 (1979)].

[36] C. Carbillet, S. Caprara, M. Grilli, C. Brun, T. Cren, F. Debontridder, B. Vignolle, W. Tabis, D. Demaille, L. Largeau, K. Ilin, M. Siegel, D. Roditchev, and B. Leridon, Phys. Rev. B **93**, 144509 (2016).

[37] D. Das and S. Doniach, Phys. Rev. B **57**, 14440 (1998).

[38] D. Das and S. Doniach, Phys. Rev. B **60**, 1261 (1999).

[39] I. S. Beloborodov, K. B. Efetov, A. V. Lopatin, and V. M. Vinokur, Phys. Rev. Lett. **91**, 246801 (2003).

[40] I. S. Beloborodov, A. V. Lopatin, V. M. Vinokur, and K. B. Efetov, Rev. Mod. Phys. **79**, 469 (2007).

[41] J. Kinney, J. Garcia-Barriocanal, and A. M. Goldman, Phys. Rev. B **92**, 100505(R) (2015).

[42] L. G. Aslamasov and A. I. Larkin, Phys. Lett. A **26**, 238 (1968).

[43] F. Nabeshima, K. Nagasawa, A. Maeda, and Y. Imai, Phys. Rev. B **97**, 024504 (2018).

[44] B. Lei, J. H. Cui, Z. J. Xiang, C. Shang, N. Z. Wang, G. J. Ye, X. G. Luo, T. Wu, Z. Sun, and X. H. Chen, Phys. Rev. Lett. **116**, 077002 (2016).

[45] L. B. Ioffe and M. Mezard, Phys. Rev. Lett. **105**, 037001 (2010).

[46] N. Trivedi, Y. Loh, K. Bouadim, and M. Randeria, J. Phys.: Conf. Ser. **376**, 012001 (2012).

[47] B. Leridon, S. Caprara, J. Vanacken, V. V. Moshchalkov, B. Vignolle, R. Porwal, R. C. Budhani, A. Attanasi, M. Grilli, and J. Lorenzana, New J. Phys. **22**, 073025 (2020).

[48] S. Oh, T. A. Crane, D. J. Van Harlingen, and J. N. Eckstein, Phys. Rev. Lett. **96**, 107003 (2006).